Electronic Supplementary Material (ESI) for Energy & Environmental Science.

Ultrahigh Oxygen-doped Carbon Quantum Dots for Highly Efficient H_2O_2 Production *via* Two-Electron Electrochemical Oxygen Reduction

Ying Guo,[a,b] Rong Zhang,[b] Shaoce Zhang,[b] Hu Hong,[b] Yuwei Zhao,[b] Zhaodong Huang,[b] Cuiping Han,[c] Hongfei Li,[d] Chunyi Zhi [b,e*]

[a] College of Materials Science and Engineering, Shenzhen University, Shenzhen, Guangdong, 518055, China

[b] Department of Materials Science and Engineering, City University of Hong Kong, 83 Tat Chee Avenue, Kowloon, Hong Kong 999077, China

[c] Faculty of Materials Science and Engineering, Shenzhen Institute of Advanced Technology, Chinese Academy of Sciences, Shenzhen, Guangdong, 518055, China

[d] Songshan Lake Materials Laboratory, Dongguan, Guangdong 523808, China

[e] Centre for Functional Photonics, City University of Hong Kong, Kowloon 999077, Hong Kong, China

Corresponding author: Prof. Chunyi Zhi

Email: cy.zhi@cityu.edu.hk

S1. Experimental section

Synthesis of glucose-derived CQD and CS samples. 40 mL (0.1 g/mL) of aqueous D-(+)-glucose solution was transferred into a 50-mL Teflon-lined stainless-steel autoclave. Consequently, the autoclave was hydrothermally treated at 160 °C for 3 h. After cooling down to room temperature, the black-brown solution was obtained by the dialysis process for 5 days to remove residues using a dialysis membrane (2000 Da). Then, the CQDs were collected by freeze-dried process at −40 °C. The CS sample was prepared with the same process but using 0.2 g/mL glucose and under 180 °C for 18 h.

Synthesis of the rGQD sample. 2 mL GO-dispersed solution (10 mg/g, Hangzhou Gaoxi Technology Co,. Ltd) was added into 18 mL of mixture solution containing 2-propanol and water (v/v=1/1). Then, the solution was transferred into a Teflon-lined stainless-steel autoclave (20 mL) and placed in an oven at 200°C for 24 h. After naturally cooling down to room temperature, 0.5 mL of hydrazine solution (80 wt%) was added into the above solution. Then, the mixture solution was stirred for 24 hours at room temperature. Subsequently, the solution was subjected to the dialysis process for 5 days to remove residues using a dialysis membrane (2000 Da). Lastly, the rGQD sample was obtained by freeze-dried process at −40°C.

Characterization. The crystalline, morphologies and structures of the samples were investigated by field-emission scanning electron microscopy (SEM, Hitachi S-4800, 5 kV), XPS (Kratos Analytical AXIS-Ultra with monochromatic Al Kα X-ray), FTIR spectra (Bruker Hyperion FTIR spectrometer), a powder X-ray diffractometer (Cu Kα radiation source, D8, Bruker), and transmission electron microscopy (TEM, Jeol 2100F). Raman spectra were collected with a Raman spectrometer (Thermo Fischer DXR).

Electrochemical measurements

H_2O_2 selectivity measurements were carried out in a three-electrode cell by a CHI 760E workstation (Chenhua, China) with a rotating disk electrode (RRDE-3A). An RRDE with a Pt ring (disk diameter: 4 mm; ring: inner diameter: 5 mm, outer diameter: 6.5 mm), Ag/AgCl (3 M KCl), and a Pt wire were used as the working, reference, and

counter electrodes, respectively. All potentials in this work refer to RHE, E(RHE) = E(Ag/AgCl) + 0.222 + 0.059pH, where pH=7. Before electrochemical measurements, the working electrodes were polished with 50 nm Al_2O_3 powder. The catalyst ink was prepared by dispersing 5 mg of catalysts in isopropyl alcohol (450 μL), deionized water (500 μL) and 0.25% Nafion (50 μL). After ultrasonication for 30 min to form a homogeneous ink. 2 μL of ink was dropped onto the surface of the glassy carbon electrode (diameter: 4 mm). All electrochemical measurements were conducted in 0.1 M Ar/O_2-saturated KOH solution (pH=13), and the loading mass was about 80 μg/cm^2. The cyclic voltammetry (CV) and linear sweep voltammetry (LSV) were recorded with the scan rate of 10 mV/s and 10 mV/s. A potential of 1.189 V (vs RHE) was applied on the ring of the working electrode at a speed of 1,600 r.p.m. during the entire testing process.

H_2O_2 selectivity of the samples on the rotating ring-disk electrode was calculated based on the current of both disc and ring electrodes, according to the following equation:

$$n = 4 \times \frac{NI_d}{NI_d + I_r}$$

$$\%HO_2^- = 200 \times \frac{I_r}{NI_d + I_r}$$

Where I_d and I_r are disk current and ring current, respectively. N is current collection efficiency of the Pt ring, which is determined as 0.35.

Bulk H_2O_2 production. The bulk measurements were conducted with a typical H-type cell, which contains 40-mL electrolyte separated by a membrane (Nafion 117) on the electrochemical workstation. Nafion membrane was pretreated in 5 wt% H_2O_2 aqueous solution at 80 °C for 1 h and then in ultrapure water at 80 °C for another 10 min. The chronoamperometry tests were conducted at a series of applied potentials.

The H_2O_2 concentration was measured by a traditional cerium sulfate $Ce(SO_4)_2$ titration method based on the mechanism that a yellow solution of Ce^{4+} would be reduced by H_2O_2 to colorless Ce^{3+} ($2Ce^{4+} + H_2O_2 = 2Ce^{3+} + 2H^+ + O_2$). Thus, the concentration of Ce^{4+} before and after the reaction can be measured by ultraviolet-

visible spectroscopy. The H_2O_2 concentration-absorbance curve was calibrated by mixing known amount of commercial H_2O_2 solution (35 wt%) with a mixture solution containing 0.1 M H_2SO_4 and 1 mM $Ce(SO_4)_2$. The absorption at 316 nm wavelength was measured on a Cary 5000 UV-Vis-NIR spectrometer (Agilent) and used to determine the Ce^{4+}/H_2O_2 concentration. To fit the linear range of calibration curve, the electrolyte collected was further diluted by 1 to 10 times in deionized water.

Computational Details

All the computations were conducted based on the density functional theory (DFT) using the Cambridge Sequential Total Energy Package (CASTEP) code of the Masterials Studio software. The generalized gradient approximation (GGA) with the Perdew-Burke-Ernzerhof (PBE) functional were used to describe the electronic exchange and correlation effects. The kinetic-energy cutoff was set as 750 eV. The geometry optimization within the conjugate gradient method was performed with forces on each atom less than 0.05 eV/Å. An energy tolerance is 5.0×10^{-6} eV per atom, and a maximum displacement of 0.001Å was considered. As showcased in **Figure S1**, 9 carbon models with 14 hexagonal rings ended with H atoms are constructed to investigate the impact of various O-containing functional groups on the adsorption behaviors of the 2eORR intermediates.

S2. Figures and tables

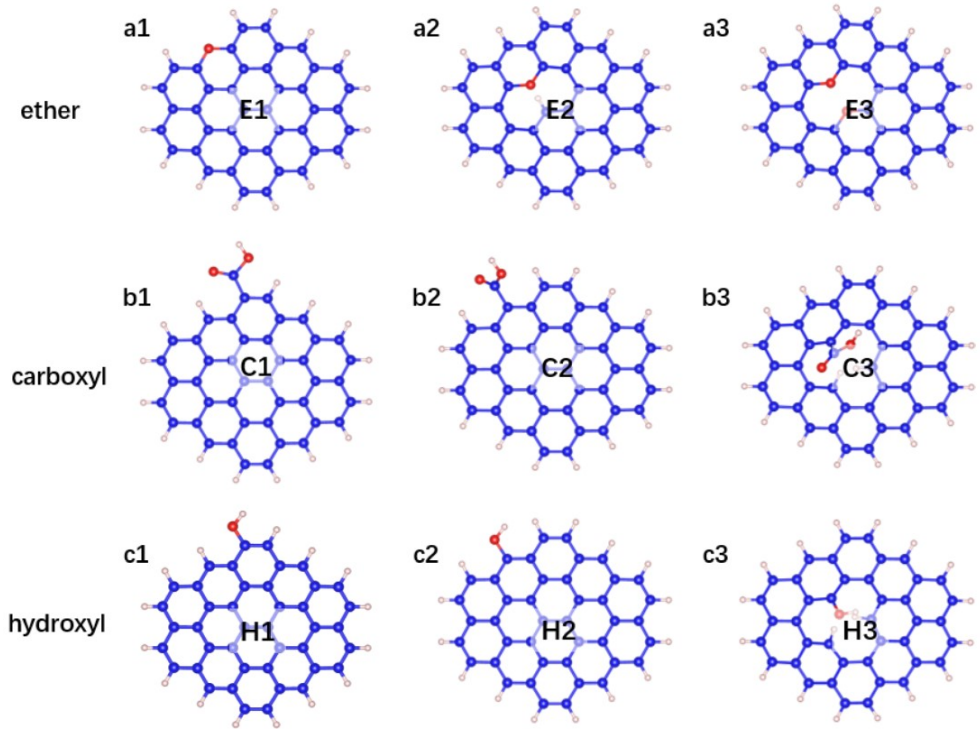

Figure S1. Optimized O-doped carbon models with various O-containing groups; (a1-a3) ether-doped models, (b1-b3) carboxyl-doped models, and (c1-c3) hydroxyl-doped models. Blue: C atom, white: H atom, red: O atom.

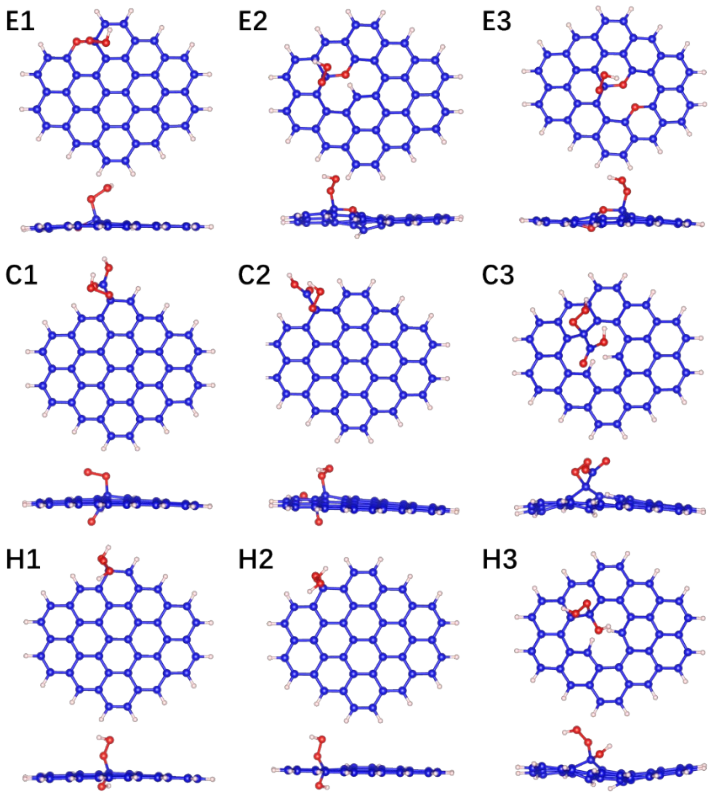

Figure S2. Various carbon configurations with the OOH intermediate adsorbed on the active sites. Blue: C atom, white: H atom, red: O atom.

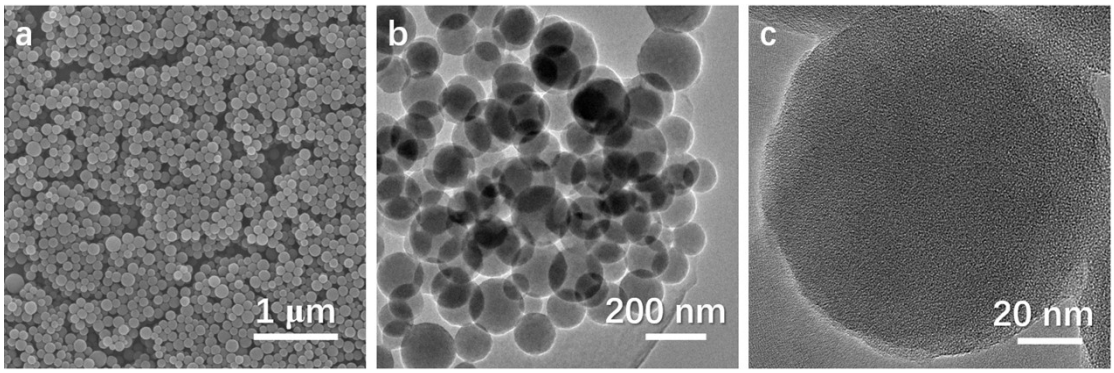

Figure S3. SEM and TEM images of the CS sample obtained by using the same method as the CQD but at 180°C for 18 h.

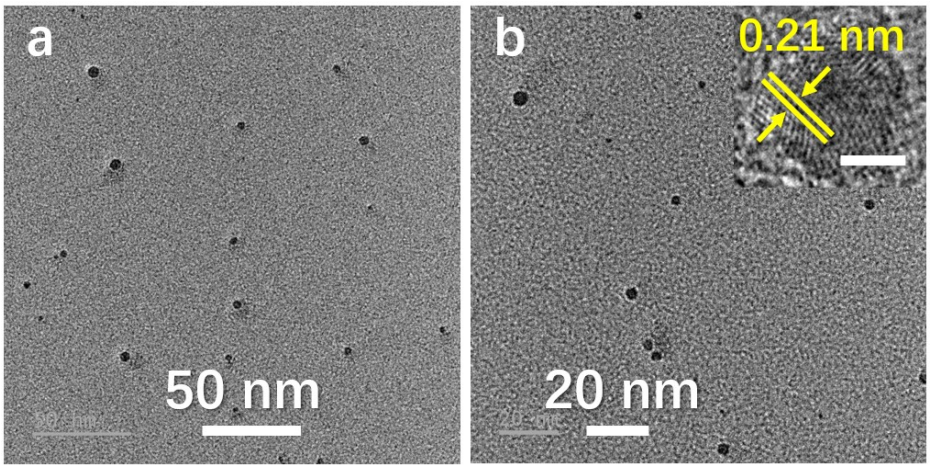

Figure S4. TEM images of the rGQD sample. Scale bar: 2 nm.

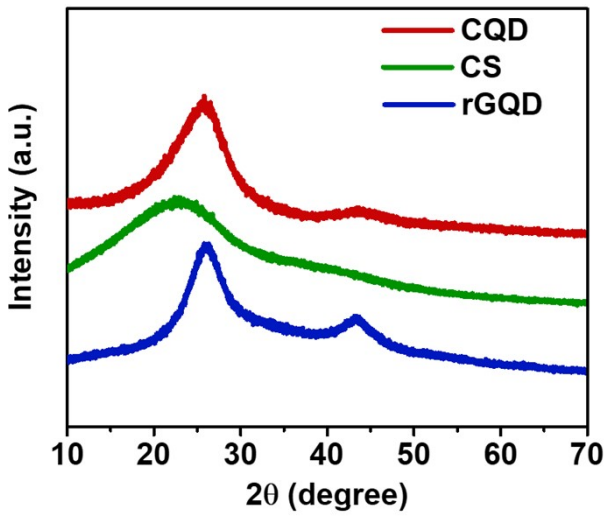

Figure S5. XRD patterns of the as-prepared samples.

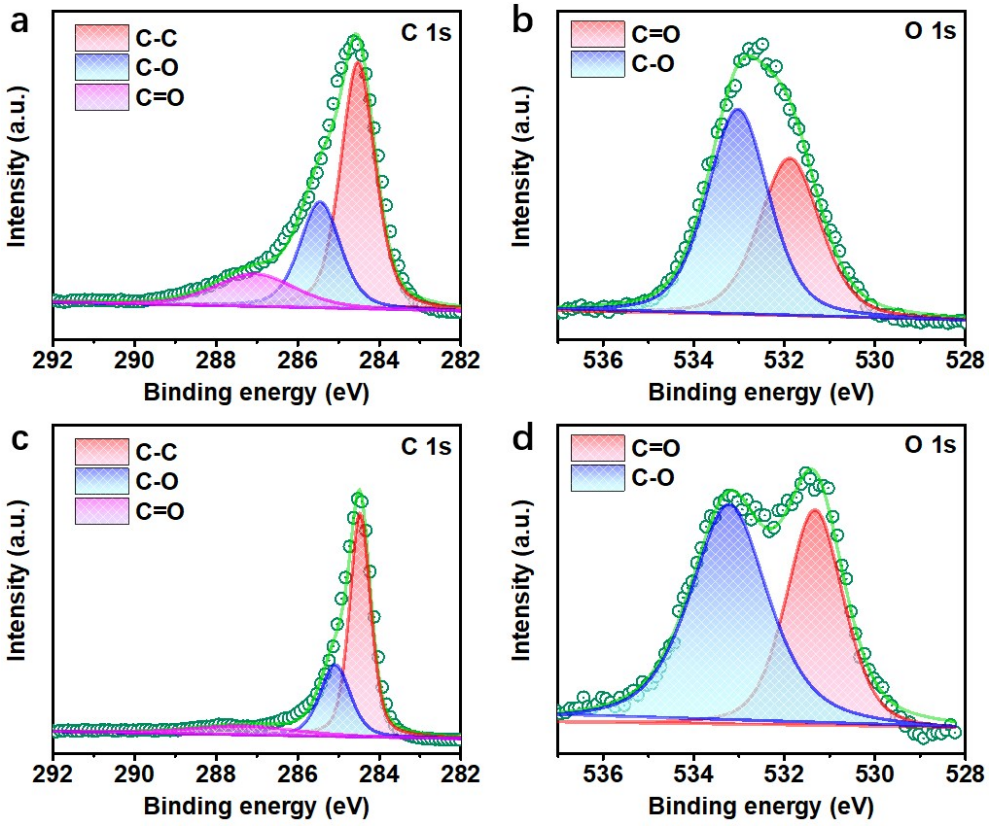

Figure S6. The C 1s and O 1s spectra of the CS (a-b) and the rGQD (c-d).

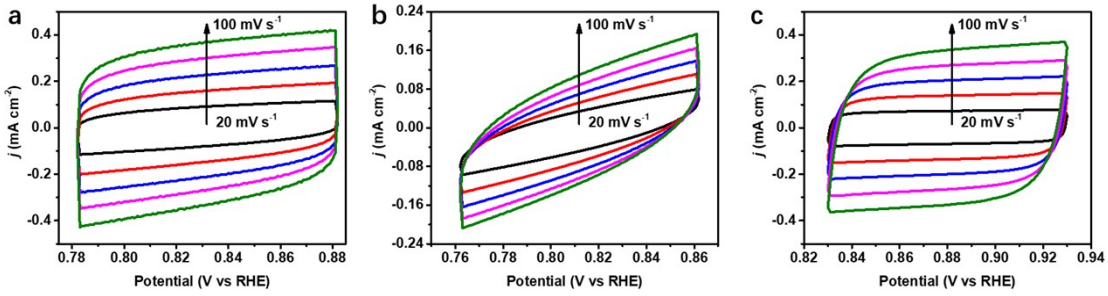

Figure S7. CV curves of the CQDs, the CSs, and the rGQDs acquired at different scan rates in the Ar-saturated 0.1 M KOH solution. The ECSA is estimated from the electrochemical double-layer capacitance of the catalytic surface. The double layer capacitance (*C*dl) has been calculated based on the plot of current density against scan rate. ECSA of working electrode can be calculated according to the equation:

$$\mathrm{ECSA}=R_{\mathrm{f}}\times S$$

where S is generally equal to the geometric area of electrode (in this work, S = 0.1256 cm^{-2}). R_f is the roughness factor of working electrode and determined by the relation: R_f=Cdl/40 μF cm^{-2}.

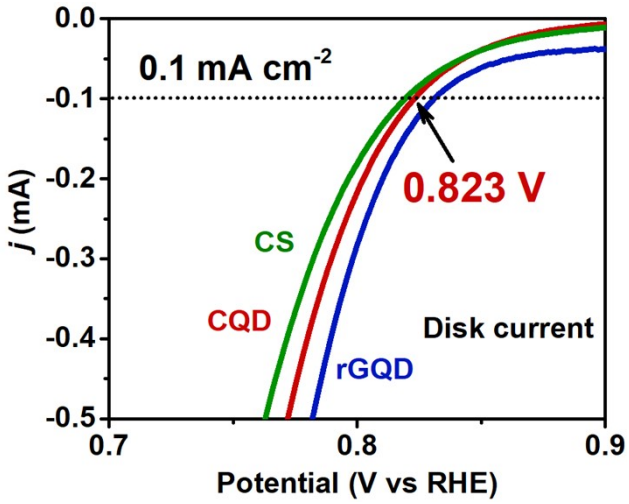

Figure S8. The enlarged area for the RRDE polarization curves that indicates the high onset potential of 0.823 V of the CQD catalyst for H_2O_2 production.

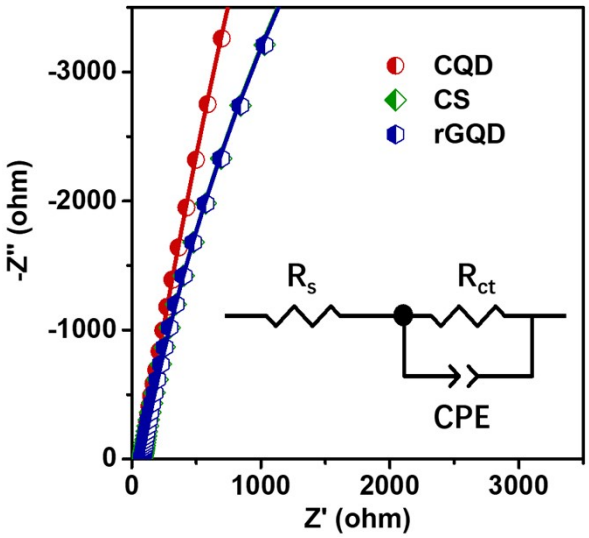

	R_s (Ω)	R_{ct} (Ω)
CQD	75.55	107.71
CS	77.52	31.78
rGQD	77.54	30.94

Figure S9. EIS curves of the as-prepared samples and the corresponding simulated parameters. EIS measurements were carried out in the frequency range from 0.1 Hz to 10^5 Hz with 5 mV amplitude in the Ar-saturated KOH electrolyte, using catalyst-modified RRDE electrode. All EIS spectra present a typical carbon feature, containing the electrolyte resistance (R_s) and a charge-transfer resistance (R_{ct}) in parallel to a constant phase element (CPE). In general, a low R_{ct} indicates a fast charge transfer between the catalyst surface and intermediates. As shown in **Figure S9**, three samples have the same *Rs*, but CQD has the largest R_{ct} value and rGQD has the smallest R_{ct} value because of their different high O contents.

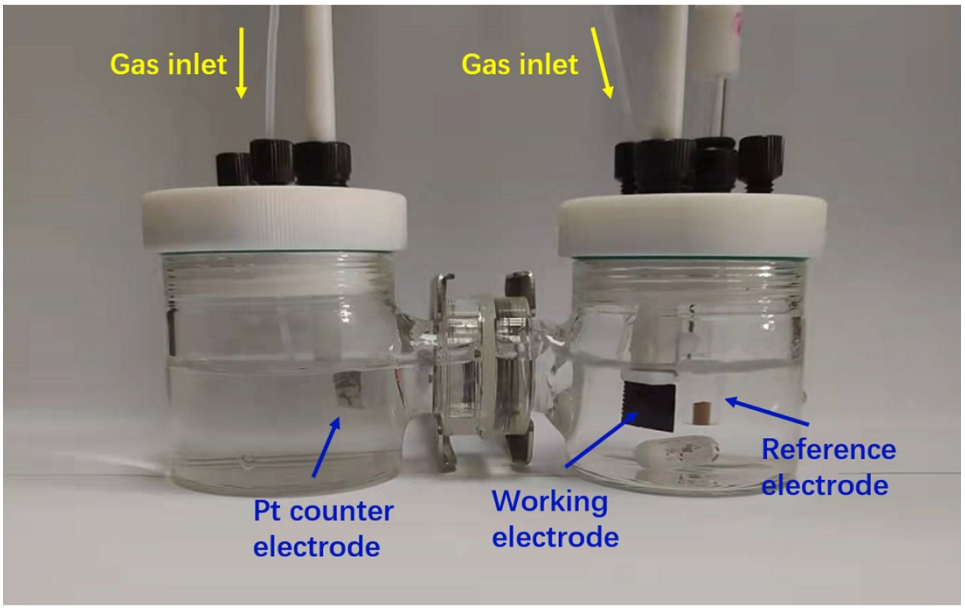

Figure S10. The photograph of the H-type cell configuration.

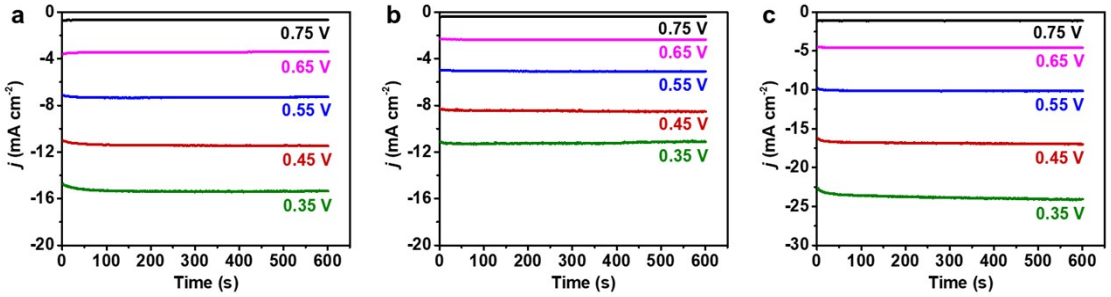

Figure S11. CA curves obtained at various applied potentials in the O_2-saturated electrolyte for the CQD (a), the CS (b), and the rGQD (c).

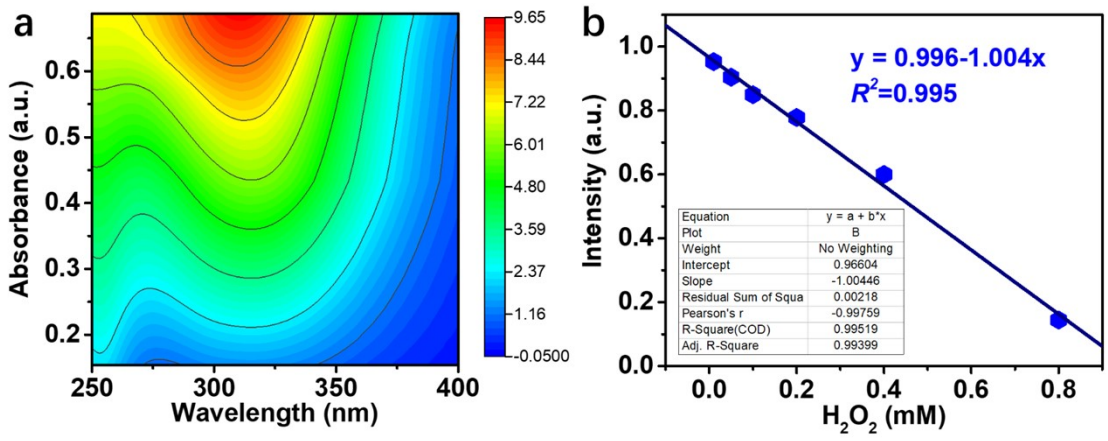

Figure S12. (a) Contour map of UV-vis absorption spectra and (b) concentration-absorbance calibration curve of H_2O_2 with the given concentrations.

Table S1. Comparison of O content of the as-prepared samples with previous works.

Catalysts	O content (%)	H_2O_2 selectivity (%)	Ref.
CQD	**0.304**	**97.5**	**This work**
OCB-PAA	0.1512	94.7	Chem 2020, 6, 1443–1458 (Ref. 7)
O-GOMC	0.13	90.0	Chem 2021, 7, 3114–3130 (Ref. 30)
O-CNTs	0.082	90.0	Nat. Catal. 2018, 156–162 (Ref. 19)
Ox-CNHs	0.0549	94.5	Chem 2018, 4, 106–123 (Ref. 17)
aCB60	0.0413	94.0	ACS Appl. Mater. Interfaces 2018, 10, 31855 (Ref. 31)

Table S2. Comparison of the H_2O_2 production in terms of H_2O_2 FE and yield recorded with H-type cell configuration.

Catalyst	Electrolyte	H_2O_2 FE (%)	Yield/mg cm^{-2} h^{-1}	Ref.
CQD	**0.1 M KOH**	**97.7**	**10.064**	**This work**
O-GOMC	0.1 M KOH	99.0	1.900	Chem 2021, 7, 3114–3130 (Ref. 30)
Pd-OCNT	0.1 M $HClO_4$	86.0	6.660	Nat. Commun. 2020, 11, 2178 (Ref. 12)
Co-N-C	0.5 M H_2SO_4	80.0	13.60	J. Am. Chem. Soc. 2019, 141, 12372–12381 (Ref. 34)
N-CHNs	0.1 M KOH	98.0	1.122	Chem 2018,4, 106-123 (Ref. 17)
MNC-600	0.1 M $KHCO_3$	88.7	0.147	ChemElectroChem 2022, 9, e202101336 (Ref. 27)
NCMK3IL50_800T	0.1 M KOH	70.0	0.955	ACS Catal. 2018, 8, 2844–2856 (Ref. 28)
Co-POC-O	0.1 M KOH	8.56	2.980	Adv. Mater. 2019, 1808173 (Ref. 41)
oxo-G/$NH_3 \cdot H_2O$	0.1 M KOH	82.0	0.762	ACS Catal. 2019, 9, 2, 1283–1288 (Ref. 32)
PIN film	$LiCLO_4$	95.0	0.159	J. Electrochem. Soc. 2020, 167, 086502 (Ref. 44)
HPC-H24	0.5 M H_2SO_4	95.0	8.070	Angew. Chem. Int. Ed., 2015, 54, 6837-6841 (Ref. 45)
O-CNTs	0.1 M KOH	92.0	0.194	J. Materiomics, 2022, 8, 136-143 (Ref. 48)
O-BC-2-650	0.1 M KOH	98.0	2.800	Sci. China Mater., 2022, 65, 1276-1284 (Ref. 51)